Computers and Geosciences 122 (2019) 1–14

Contents lists available at ScienceDirect

Computers and Geosciences

journal homepage: www.elsevier.com/locate/cageo

Research paper

Finite-element modelling of glacial isostatic adjustment (GIA): Use of elastic foundations at material boundaries versus the geometrically non-linear formulation

Andrea Hampel[a,*,1], Jens Lüke[b,2], Thomas Krause[c,3], Ralf Hetzel[d,4]

[a] Institut für Geologie, Leibniz Universität Hannover, Callinstr. 30, 30167 Hannover, Germany
[b] Simulia EuroCentral CoE, Dassault Systèmes, Elisabethstr. 16, 52062 Aachen, Germany
[c] Institut für Informationsverarbeitung, Leibniz Universität Hannover, Appelstr. 9A, 30167 Hannover, Germany
[d] Institut für Geologie und Paläontologie, Westfälische Wilhelms-Universität Münster, Corrensstr. 24, 48149 Münster, Germany

ARTICLE INFO

Keywords:
Finite-element modelling
Glacial isostatic adjustment
Elastic foundation
ABAQUS
Geodynamic modelling

ABSTRACT

Commercial finite-element software packages like ABAQUS are widely used for geodynamic modelling, which usually requires considering isostatic effects, for example, to calculate displacements and stresses resulting from glacial isostatic adjustment (GIA). Since Wu (Geophysical Journal International, 158, 401–408, 2004) proposed that models created with commercial finite-element software need to implement elastic ("Winkler") foundations at all external and internal material boundaries to account for restoring forces, this approach has been applied by many GIA and other geoscientific studies. However, there is no consensus about the necessity of implementing elastic foundations, which have the disadvantage that the stress output needs post-processing to obtain meaningful results. Here we demonstrate that the elastic-foundation approach was derived from an Eulerian formulation of the equation of motion for elastic and viscoelastic materials. Finite-element codes like ABAQUS, however, use a Lagrangian formulation, which renders the implementation of elastic foundations at all material boundaries unnecessary if the geometrically non-linear formulation (NLGEOM) is used. Results from viscoelastic half-space models show that for incompressible viscoelastic materials models with elastic foundations (but no NLGEOM) and models with NLGEOM (but no elastic foundations) yield vertical displacements underneath the load that differ by less than 1% from the analytical solution. Both models reach a state of isostatic equilibrium. In contrast, models without NLGEOM and elastic foundations do not reach isostatic equilibrium, i.e. the model surface continuously subsides under the load. Models with both NLGEOM and elastic foundations behave overly stiff and yield wrong displacement fields. Results from models based on Archimedes' principle demonstrate that restoring forces are correctly calculated when using NLGEOM, which has the advantage that the stress output can be used without post-processing and that negative density contrasts (e.g. between salt and surrounding rocks) can be taken into account within the model domain, which is impossible when using elastic foundations.

1. Introduction

Many geoscientific applications of numerical codes require the incorporation of isostatic effects to simulate, for example, the behaviour of the crust or lithosphere during deformation (e.g. Bird, 1978; King and Ellis, 1990; Wdowinski and Axen, 1992). Thereby, the modeller usually faces the problem that the region of interest is much smaller than the model domain that would actually be needed to compute the isostatic compensation in the sub-lithospheric layers. To overcome this problem, elastic foundations (also called “Winkler foundations”) were introduced as a way to simulate isostatic effects without the need to include the layer beneath the region of interest into the model (Fischer et al., 2004; Fourel et al., 2014; Hampel et al., 2009; Henk, 2006; Kurfeß and Heidbach, 2009; Lester et al., 2012; McMullen et al., 1981;

* Corresponding author.
E-mail address: hampel@geowi.uni-hannover.de (A. Hampel).
[1] Author contribution: designed the study, ran and analysed the models, drafted and revised the manuscript and acted as corresponding author.
[2] Author contribution: developed the theoretical concept, contributed to the model design and analysis, edited and revised the manuscript.
[3] Author contribution: performed the inverse Fourier transformation, edited and revised the manuscript.
[4] Author contribution: contributed to model analysis and interpretation, edited and revised the manuscript.

https://doi.org/10.1016/j.cageo.2018.08.002
Received 11 October 2017; Received in revised form 24 July 2018; Accepted 9 August 2018
Available online 11 August 2018
0098-3004/

Williams and Richardson, 1991). Elastic foundations simulate the restoring forces arising from the density contrast between the lowermost model layer and a virtual layer underneath, which is not part of the finite-element mesh (e.g. ABAQUS 6.14 documentation). The stiffness of the foundation (vertical stress per vertical displacement) is the product of the density of the foundation and acceleration due to gravity. This approach is consistent with modelling uplift of a body submerged in a fluid. A typical application is the simulation of the asthenosphere as a virtual layer underneath the model lithosphere to consider isostatic effects arising, for example, from mass re-distributions or loading/unloading of the model surface (Hampel et al., 2009; Kurfeß and Heidbach, 2009; McMullen et al., 1981; Turpeinen et al., 2008; Watts, 2001).

While the use of elastic foundations at the model bottom is a standard approach, there is a long-standing debate on the necessity of incorporating elastic foundations at all material boundaries with a density contrast, including the model surface and internal boundaries (Bängtsson and Lund, 2008; Hampel et al., 2009; Schmidt et al., 2012; Williams and Richardson, 1991; Wu, 1992, 2004). This approach was introduced by Wu (1992) and described in more detail by Wu (2004) for the use in the software package ABAQUS. Wu (2004) argued that elastic foundations are necessary because he found that commercial finite-element software codes do not track the stress initially introduced by the gravity field and hence neglect restoring forces at internal and external material boundaries. To activate the restoring forces, Wu (2004) suggested to define elastic foundations at all material boundaries, with a value calculated from the density contrast between the layers. As shown by Wu (1992), only models with elastic foundations yielded vertical displacements under loading in agreement with analytical solutions. In models without elastic foundations, the surface sinks under the load without reaching isostatic equilibrium. The elastic-foundation approach should be employed in models with and without gravity, regardless if the material is incompressible or compressible (Lund, 2005; Steffen et al., 2006; Steffen, 2013). As an advancement of Wu (2004)'s approach, Schmidt et al. (2012) suggested to define spring elements at each node along the material boundary instead of elastic foundations because this allows accounting for inclined boundaries.

Wu (1992, 2004)'s approach has widely been applied in GIA simulations (Lund, 2005; Schotman et al., 2008, 2009; Steffen et al., 2006, 2014a, b; van der Wal et al., 2013; Wang and Wu, 2006; Wu, 2005) but also in other studies on, for example, deformation of continental interiors (Martin-Velazquez and de Vicente, 2012) or lithospheric flexure on Mars (Musiol et al., 2016). However, it has two main disadvantages. First, internal elastic foundations perturb the stress field in the model, with the consequence that the computed stresses must be post-processed to obtain correct values by adding the product of density, vertical displacement and gravitational acceleration to the diagonal components of the stress tensor output from ABAQUS (Wu, 2004). For models that require an undisturbed stress field prior to post-processing to correctly calculate, for example, the shear and normal stresses on a fault, this poses a serious problem. Second, negative density contrasts at internal material boundaries cannot be taken into account, because ABAQUS does not allow defining negative foundation stiffnesses. This precludes, for example, the incorporation of salt layers or an asthenosphere with a lower density than the lithospheric mantle.

In Section 2, we show that the apparent need of using elastic foundations at all material boundaries with density contrasts stems from an Eulerian formulation of the underlying equations, which contain a term for pre-stress advection. In a Lagrangian formulation, this term is not required, which raises the question why elastic foundations should be implemented in Lagrangian finite-element codes like ABAQUS. We show that elastic foundations are only needed if Lagrangian models are run with the so-called “small-displacement" approach, whereas they are unnecessary in a geometrically non-linear, “large-displacement" analysis. In Section 3, we present viscoelastic half-space models with a setup after Wu (1992) and models representing a column of solid material floating on an inviscid fluid to investigate how elastic foundations affect the results of small and large displacement analyses.

2. Eulerian versus Lagrangian formulation of underlying equations

When introducing his approach of using elastic foundations, Wu (2004) referred to equation II-22 in Cathles (1975), which is the equation of motion for an elastic material:

$$\vec{\nabla}\cdot\bar{\bar{\tau}} - \vec{\nabla}(\vec{u}\cdot\rho_0 g_0 \hat{r}) - \rho_1 g_0 \hat{r} - \rho_1 \vec{\nabla}\phi_1 = 0 \quad (1)$$

where $\bar{\bar{\tau}}$ is the stress tensor, $\vec{u}$ is the displacement vector, $\hat{r}$ is the unit vector in the radial direction and ρ, g, ϕ are density, gravitational acceleration and gravitational potential, respectively. The subscript zero refers to the hydrostatic stress state, while the subscript one refers to the perturbed stress state. The first term of equation (1) is the divergence of stress, which also appears in the stiffness equation ($\vec{\nabla}\cdot\bar{\bar{\tau}} = 0$) solved by commercial finite-element packages. By the third and fourth terms, potential effects from internal buoyancy (for example, density changes arising from material compressibility) and self-gravitation can be included.

Wu (2004)'s approach is based on the second term, which accounts for the so-called “pre-stress advection”. This term ensures that particles with an initial lithostatic stress (caused by the initial gravity field) carry this stress with them when they are displaced during deformation. The pre-stress advection term is linked to the restoring force of isostasy. Without this term, there will be no viscoelastic gravitational relaxation and any mass left on the surface of the Earth will sink to the centre resulting in a singular solution at large model times (Wu, 2004). As the stiffness equation $\vec{\nabla}\cdot\bar{\bar{\tau}} = 0$ solved by commercial finite-element codes does not contain the pre-stress advection term, Wu (1992, 2004) proposed to introduce elastic foundations at all material boundaries to include pre-stress advection and isostatic restoring forces. The value of each elastic foundation should be given by the user as the density contrast across the layers times gravitational acceleration. As internal elastic foundations modify the stress field, the computed stresses must be post-processed by adding the product of density, vertical displacement and gravitational acceleration to the diagonal components of the stress tensor output from ABAQUS. In contrast, the modelled displacements should not be affected by adding elastic foundations to a model (Wu, 2004).

Inspection of Cathles (1975) reveals that equation (1) is based on an Eulerian formulation. In an Eulerian formulation, particles move relative to the initially defined geometry, which remains unchanged during deformation. As particles do not carry the information about the initial hydrostatic stress with them, an additional terms is required for pre-stress advection (Cathles, 1975; Love, 1911). This advection term in general relates the material derivative of a field to its local derivative. The total stress at the position of each particle needs to be determined from the stress gradient in the model. In a Lagrangian formulation, however, the material is coupled to the geometry and they deform together. As each particle carries the information about its initial position and stress with it, the pre-stress advection term is not needed to determine the total stress for each particle. Hence, pre-stress advection and buoyancy forces may be included in a Lagrangian formulation, i.e. no additional terms are required for their implementation.

Commercial finite-element codes like ABAQUS are based on the Lagrangian formulation, which raises the question why it should be necessary to account for pre-stress advection by additional boundary conditions such as elastic foundations or spring elements. The answer to this question is related to the fact that there are two fundamentally different approaches to treat the relationship between the material and the initial mesh geometry: Lagrangian analyses may be run with or without the so-called “geometrically non-linear formulation” (named NLGEOM in ABAQUS). Without this formulation, the software applies the small-displacement approach, i.e. the finite elements are formulated relative to the initial geometry, using initial nodal coordinates, and the kinematic relationships are linearised (ABAQUS 6.14 documentation). In a small-displacement analysis, the infinitesimal strain measure is used. The consequences of this infinitesimal strain approximation for modelling isostatic effects were described by Williams and Richardson (1991) (bold font added by authors of present study): "*Any uplift that occurs as a result of tectonic forces must be countered by isostatic forces proportional to the amount of uplift. If this were not true, tectonic uplift could continue indefinitely, resulting in infinite topography. Ordinarily, this would be the case in time-dependent finite element calculations, with or without the use of body forces. At each time step, uplift would proceed in a manner dictated by the present set of forces, regardless of the amount of uplift that had occurred in the previous time step.* ***This is a result of the infinitesimal strain approximation used in most finite element calculations. All spatial quantities are referenced to the initial nodal positions, so that the entire grid geometry remains unchanged over the course of the calculations.*** *Therefore, no matter how much vertical uplift has been induced by the applied boundary conditions, the system of body forces will be the same as it was initially.*" In other words, pre-stress advection and restoring forces are not taken into account in the Lagrangian small-displacement approach.

Apart from the infinitesimal strain approximation, ABAQUS offers – since its first version published in 1978 – the possibility of a geometrically non-linear (NLGEOM) analysis. This kind of analysis represents the “large-displacement" approach, in which the elements are formulated in the current geometry using the current nodal positions; the calculated stress at each point is the “true” (Cauchy) stress, which results from the deformation history of the respective element (ABAQUS 6.14 documentation). In other words, each particle carries the information about the stress with it, i.e. there is no need to account for pre-stress advection by elastic foundations. More importantly, it remains hitherto unexplored how elastic foundations affect the modelled displacement and stresses when they are used in an NLGEOM analysis (e.g. Steffen, 2013).

The basic finite element equations used in ABAQUS are given in integral form in the Abaqus 6.14 documentation. In addition to the geometrically nonlinear stiffness matrix, they include the initial stress matrix, describing stress-stiffening effects, and the load stiffness matrix, describing the deformation-dependency of loads such as the dependency of gravity loading on the momentary density (internal buoyancy). Self-gravitation, however, is not included.

Note that the ABAQUS documentation recommends – since at least version 6.3, which was used by Hetzel and Hampel (2005) – the use of NLGEOM for models containing sources of geometrical non-linearity, such as contact interfaces to simulate faulting. Note that also all later models by Hampel and co-workers were run with NLGEOM and hence included pre-stress advection and buoyancy forces (e.g. Hampel and Hetzel, 2006; Hampel et al., 2007, 2009, 2010; Turpeinen et al., 2008). In the next section, we evaluate the effect of using elastic foundations in models with and without NLGEOM on the model results.

3. Model sets for evaluating NLGEOM versus elastic foundations

To evaluate the two approaches – geometrically non-linear (NLGEOM) analysis versus elastic foundations at all material boundaries – we computed a series of models with a deliberately simple setup. The first two model sets represent an incompressible viscoelastic half-space with the same parameters as used by Wu (1992). The modelled displacements during loading are compared with the analytical solution (Wolf, 1985; Wu, 1992, his Appendix A). The third model set comprises a column floating on an inviscid fluid to evaluate how elastic foundations affect the modelled displacement and stress fields for compressible and incompressible as well as for elastic and viscoelastic materials. The naming of the models is summarized in Table 1. All models were run using ABAQUS/Standard version 6.14. To show that our conclusions are also valid for an older and the most recent ABAQUS version, we ran all Haskell-type and floating-column models with versions 6.7 (published 2007; Figs. S1, S2) and 2017 (published 2017; Figs. S3, S4).

3.1. Incompressible viscoelastic half-space models after Wu (1992)

Wu (1992) presented two incompressible viscoelastic half-space models with a boxcar (or Heaviside) load to show the validity of the finite-element approach for GIA modelling. The first model (Wu, 1992; his Fig. 1a) simulated the loading of a viscoelastic half-space with the same parameters as used by Haskell (1936), who provided an analytical solution for the loading of a viscous half-space. For the comparison between finite-element results and analytical solution, Wu (1992; his Fig. 1a) used the solution for Heaviside loading of a viscoelastic half-space provided by Wolf (1985). In the following, we refer to these models as Haskell-type models (Fig. 1a; Table 1). The second model (Wu, 1992; his Fig. 2) had the same setup but the material density was changed and unloading of the half-space was also considered. We hereafter refer to these models as Wu92-Fig2-type models (Fig. 1b). In the following, we describe the models in more detail and use them for comparing the two different approaches (NLGEOM and elastic foundations). For each setup, we computed four models (Table 1). Note that the model name indicates the applied approach (*_E: with elastic foundation; *_N: with NLGEOM; *_noNE: without NLGEOM or elastic foundation; *_N + E: with both, elastic foundation and NLGEOM). For the loading phases, we compare the vertical surface displacement against the solution given by Wolf (1985).

3.1.1. Setup and results from Haskell-type models

Our Haskell-type models (Fig. 1a) are 60000 × 60000 km large and meshed with 25 × 25 km large linear, rectangular plane strain elements suitable for incompressible materials (CPE4H). By using these model dimensions and element edge lengths, we follow the recommendations given in Wu and Johnston (1998) for obtaining results with a deviation of less than 1% underneath the load compared to the analytical solution. On top of the model, a 1000-km-wide load with a magnitude of 15 MPa is applied instantaneously. In the models Haskell_E and Haskell_N + E, an elastic foundation is applied to the model surface (Table 1).

The models were computed as a sequence of four analysis steps. In the first step (ABAQUS Keyword *Static), in which only elastic material behaviour is taken into account, gravity is applied and a lithostatic stress field is established (Ellis et al., 2006; Fischer, 2001; Hampel et al., 2009; Hergert et al., 2015). To facilitate the calculation, we define the lithostatic stress field as initial condition (*Initial conditions, type = stress, geostatic) (ABAQUS 6.14 documentation). In the second step (*Visco), viscoelastic behaviour is switched on and the viscoelastic material is allowed to equilibrate under gravity for 10 ka. This

Table 1
Overview of the models used to evaluate the use of non-linear geometry analysis (NLGEOM) versus elastic foundations.

Model	Elastic foundation	NLGEOM	Gravity	Material	
Haskell-type models					
Haskell_N	–	x	x	viscoelastic	incompressible
Haskell_E	x	–	x	viscoelastic	incompressible
Haskell_noNE	–	–	x	viscoelastic	incompressible
Haskell_N + E	x	x	x	viscoelastic	incompressible
Wu92-Fig2-type models					
Wu92-Fig2_N	–	x	x	viscoelastic	incompressible
Wu92-Fig2_E	x	–	x	viscoelastic	incompressible
Wu92-Fig2_noNE	–	–	x	viscoelastic	incompressible
Wu92-Fig2_N + E	x	x	x	viscoelastic	incompressible
Floating column models					
C1-3-i-e_N,C2-2-i-e_N	–	x	–	elastic	incompressible
C1-3-i-ve_N, C2-2-i-ve_N	–	x	–	viscoelastic	incompressible
C1-3-i-e-g_N, C2-2-i-e-g_N	–	x	x	elastic	incompressible
C1-3-i-ve-g_N, C2-2-i-ve-g_N	–	x	x	viscoelastic	incompressible
C1-3-i-e_E, C2-2-i-e_E	x	–	–	elastic	incompressible
C1-3-i-ve_E, C2-2-i-ve_E	x	–	–	viscoelastic	incompressible
C1-3-i-e-g_E, C2-2-i-e-g_E	x	–	x	elastic	incompressible
C1-3-i-ve-g_E, C2-2-i-ve-g_E	x	–	x	viscoelastic	incompressible
C1-3-c-e_N, C2-2-c-e_N	–	x	–	elastic	compressible
C1-3-c-ve_N, C2-2-c-ve_N	–	x	–	viscoelastic	compressible
C1-3-c-e-g_N, C2-2-c-e-g_N	–	x	x	elastic	compressible
C1-3-c-ve-g_N C2-2-c-ve-g_N	–	x	x	viscoelastic	compressible
C1-3-c-e_E, C2-2-c-e_E	x	–	–	elastic	compressible
C1-3-c-ve_E, C2-2-c-ve_E	x	–	–	viscoelastic	compressible
C1-3-c-e-g_E, C2-2-c-e-g_E	x	–	x	elastic	compressible
C1-3-c-ve-g_E, C2-2-c-ve-g_E	x	–	x	viscoelastic	compressible

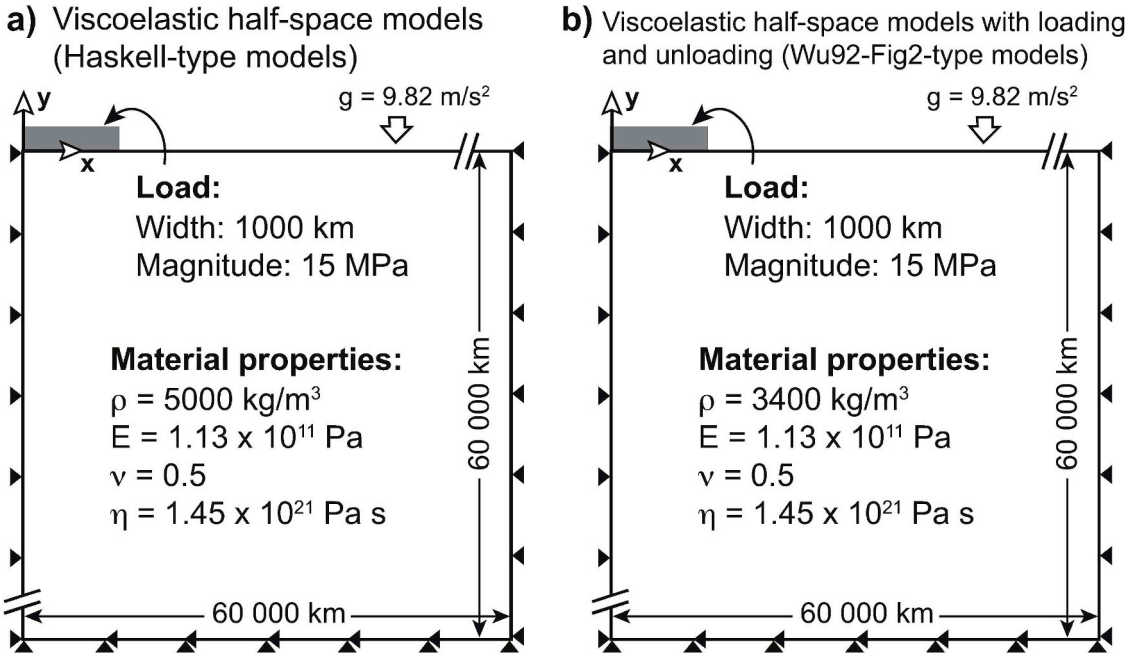

Fig. 1. Model setups. a) Viscoelastic Haskell-type half-space models. b) Viscoelastic Wu92-Fig2-type half-space models used for modelling loading and subsequent unloading (after Wu, 1992; his Fig. 2). Both model types are meshed with 25 × 25 km large linear, rectangular plane strain elements suitable for incompressible materials (CPE4H). The same mesh and element type are used in all model runs. All viscoelastic half-space models (i.e. with and without elastic foundations and/or NLGEOM) have the same boundary conditions (indicated by black triangles): the model bottom is fixed in both the vertical and horizontal direction while the model sides are fixed in the horizontal direction. In models with an elastic foundation (Table 1), it is applied to the model surface. Abbreviations for model parameters are ρ density, E Young's modulus, ν Poisson's ratio, η viscosity and g acceleration due to gravity. Following Wu (1992), we use a value of g = 9.82 m/s^2 in the viscoelastic half-space models. The linear viscosity of 1.45 × 10^{21} Pa s enters the model via the keyword *Creep as parameter A with a value of 2.3 × 10^{-22} Pa s. In all models, the load is applied (and removed, if applicable) instantaneously. The magnitude of the applied load is 15 MPa, which is equivalent to ~1.5 km of ice. The left end of the load coincides with the origin of the coordinate system at the beginning of the model run. See text for details.

procedure ensures that the deformation caused by applying gravity to a viscoelastic material is minimized before the load is applied. Note that these two initial steps are optional; they can be included in models of any scale, in which isostasy is to be simulated (see Appendix A for templates of ABAQUS input files). In the third step (*Visco), the load is applied; this step lasts one second and yields the elastic response. In the fourth step (*Visco), the vertical displacement of the model surface is computed at the same three time points as in Wu (1992). To compare

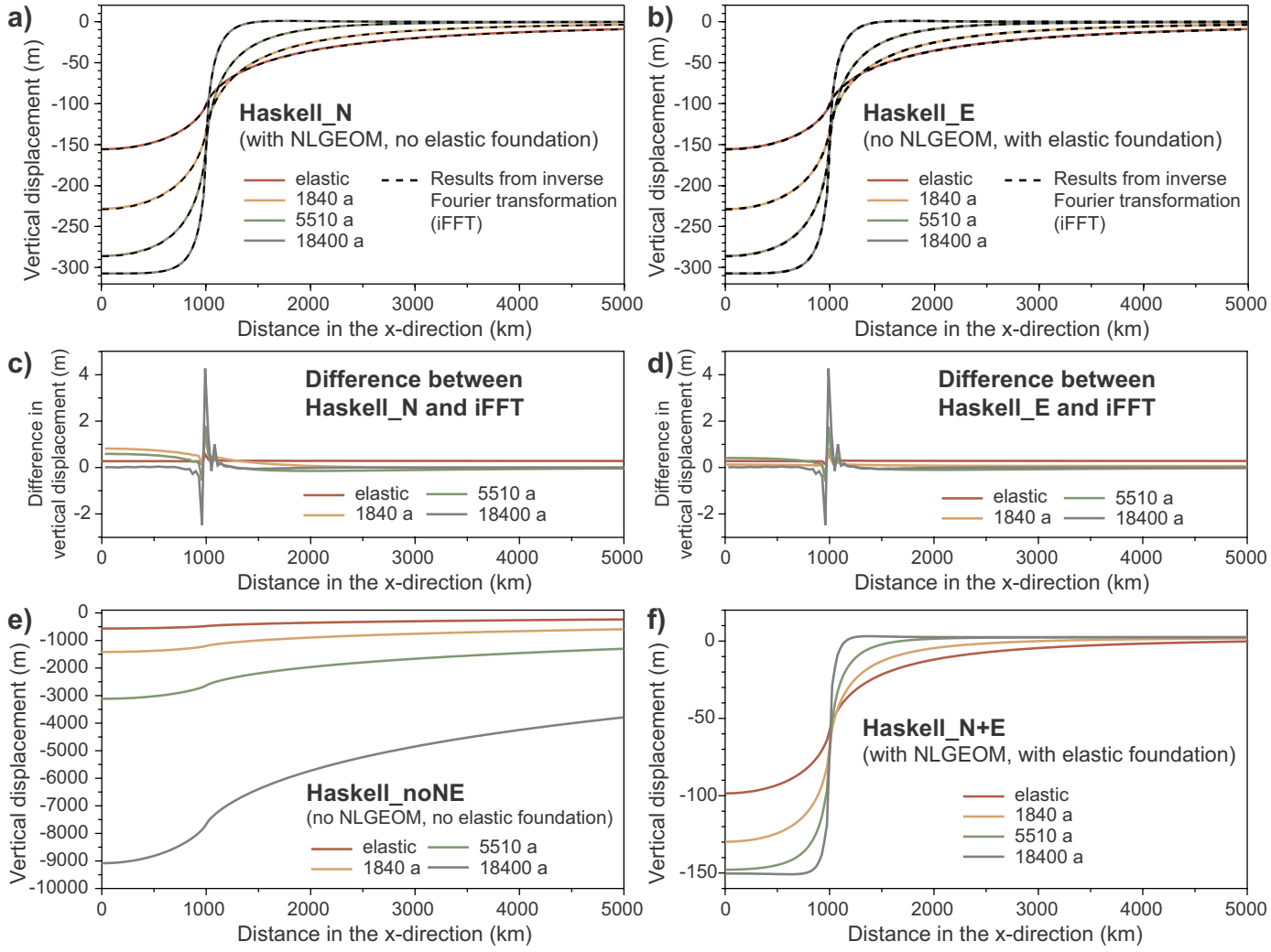

Fig. 2. Results from Haskell-type half-space models (Fig. 1a; Table 2). Diagrams in the upper row show the vertical surface displacement in the models (a) Haskell_N (with NLGEOM, no elastic foundation) and (b) Haskell_E (no NLGEOM, with elastic foundation). Dashed black lines indicate the results from the inverse Fourier transformation (iFFT) of the solution given by Wolf (1985). Diagrams in the centre row show the difference in the vertical displacement between iFFT and the models (c) Haskell_N and (d) Haskell_E, respectively. Diagrams in the lower row show the vertical displacement in the models (e) Haskell_noNE (no NLGEOM, no elastic foundation) and (f) Haskell_N + E (with NLGEOM, with elastic foundation). The vertical displacement derived from the finite-element models is given relative to the upper right corner of the mesh.

Table 2
Results of the Haskell-type models with a viscoelastic halfspace under a Heaviside load (see Figs. 1a and 2). Results of the inverse Fourier transformation of the solution given by Wolf (1985) are shown in the last row.

Model name	Elastic foundation	Non-linear geometry	Vertical displacement (m) at x = 0			
			Elastic response	1840 a	5510 a	18400 a
Haskell_N	no	yes	−155.5	−228.2	−285.8	−307.4
Haskell_E	yes	no	−155.5	−228.9	−286.0	−307.4
Haskell_noNE	no	no	−564.8	−1417	−3115	−9082
Haskell_N + E	yes	yes	−98.5	−129.8	−150.3	−150.9
inverse FFT solution	–	–	*−155.8*	*−229.0*	*−286.4*	*−307.4*

our results with the theoretical prediction, we used MATLAB to compute the vertical displacement of the surface at these different stages by inverse Fourier transformation of the solution given by Wolf (1985). The inverse Fourier transformation required the shear modulus as input, which we calculated from the Young's modulus and Poisson's ratio to be 3.7667×10^{10} Pa.

The results from the Haskell-type experiments show that both models with an elastic foundation (but no NLGEOM) and models with NLGEOM (but no elastic foundation) yield vertical displacements underneath the load that differ by less than 1% from the analytical

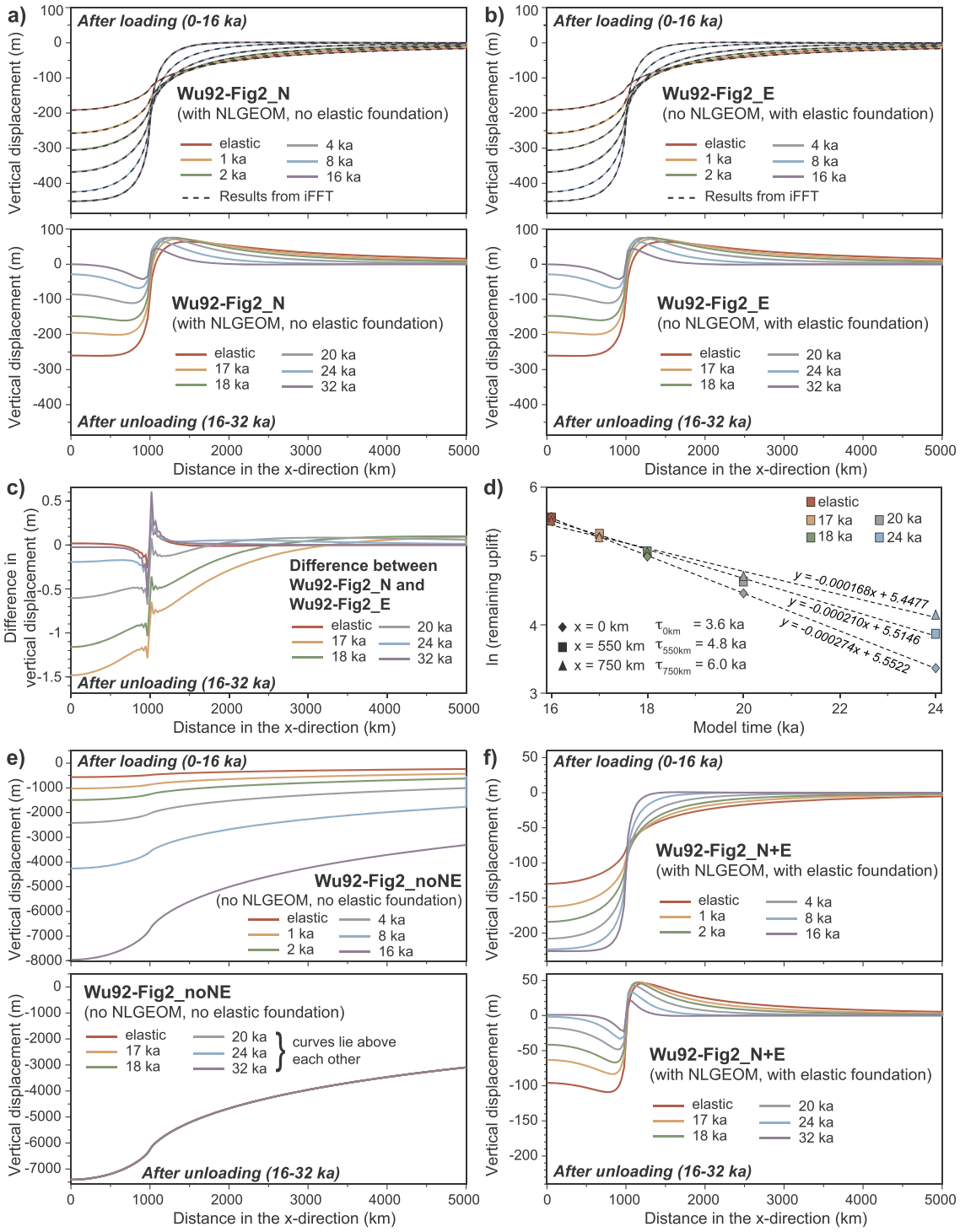

Fig. 3. Vertical surface displacement after application (0–16 ka) and removal of load (16–32 ka) obtained from the Wu92-Fig2-type half-space models (Fig. 1b; Table 3). (a) Wu92-Fig2_N (with NLGEOM, no elastic foundation). (b) Wu92-Fig2_E (no NLGEOM, with elastic foundation). Dashed black lines in the diagrams in the upper row indicate the results from the inverse Fourier transformation (iFFT) of the solution given by Wolf (1985). (c) Difference in the vertical displacement after load removal between the models Wu92-Fig2_N and Wu92-Fig2_E. (d) Semi-log plot of the remaining uplift versus the time after load removal for three different locations (x-coordinates: 0, 550 and 750 km, respectively) underneath the former load (cf. Wu, 1992; his Fig. 3). The relaxation times at these points (τ_{0km}, τ_{550km} and τ_{750km}) are determined from the slope of the regression lines, which is inversely proportional to the relaxation time. Plot is derived from model Wu92-Fig2_N; model Wu92-Fig2_E yields identical relaxation times. (e) Vertical displacements from model Wu92-Fig2_noNE (no NLGEOM, no elastic foundation). (f) Vertical displacements from model Wu92-Fig2_N + E (with NLGEOM, with elastic foundation). The vertical displacement derived from the finite-element models is given relative to the upper right corner of the mesh.

Table 3
Results of Wu92-Fig2-type models with a viscoelastic halfspace under a Heaviside load (see Figs. 1b and 3). Results of the inverse Fourier transformation of the solution given by Wolf (1985) for the phase with the load are shown in the last row.

Model name	Vertical displacement (m) at x = 0											
	Time after loading						Time after unloading					
	Elastic response	1 ka	2 ka	4 ka	8 ka	16 ka	Elastic response	1 ka	2 ka	4 ka	8 ka	16 ka
Wu92-Fig2_N	−191.1	−256.7	−304.6	−367.0	−424.1	−451.2	−260.1	−195.3	−147.9	−86.0	−28.8	−0.26
Wu92-Fig2_E	−191.1	−258.2	−305.8	−367.6	−424.3	−451.2	−260.1	−193.8	−146.7	−85.4	−28.6	−0.24
Wu92-Fig2_noNE	−564.8	−1028	−1491	−2416	−4268	−7971	−7406	−7406	−7406	−7406	−7406	−7406
Wu92-Fig2_N + E	−129.7	−162.4	−183.9	−207.8	−223.1	−225.6	−96.0	−63.1	−41.5	−17.4	−1.77	−1.00
inverse FFT solution	*−191.7*	*−257.5*	*−305.7*	*−368.1*	*−424.8*	*−451.4*	–	–	–	–	–	–

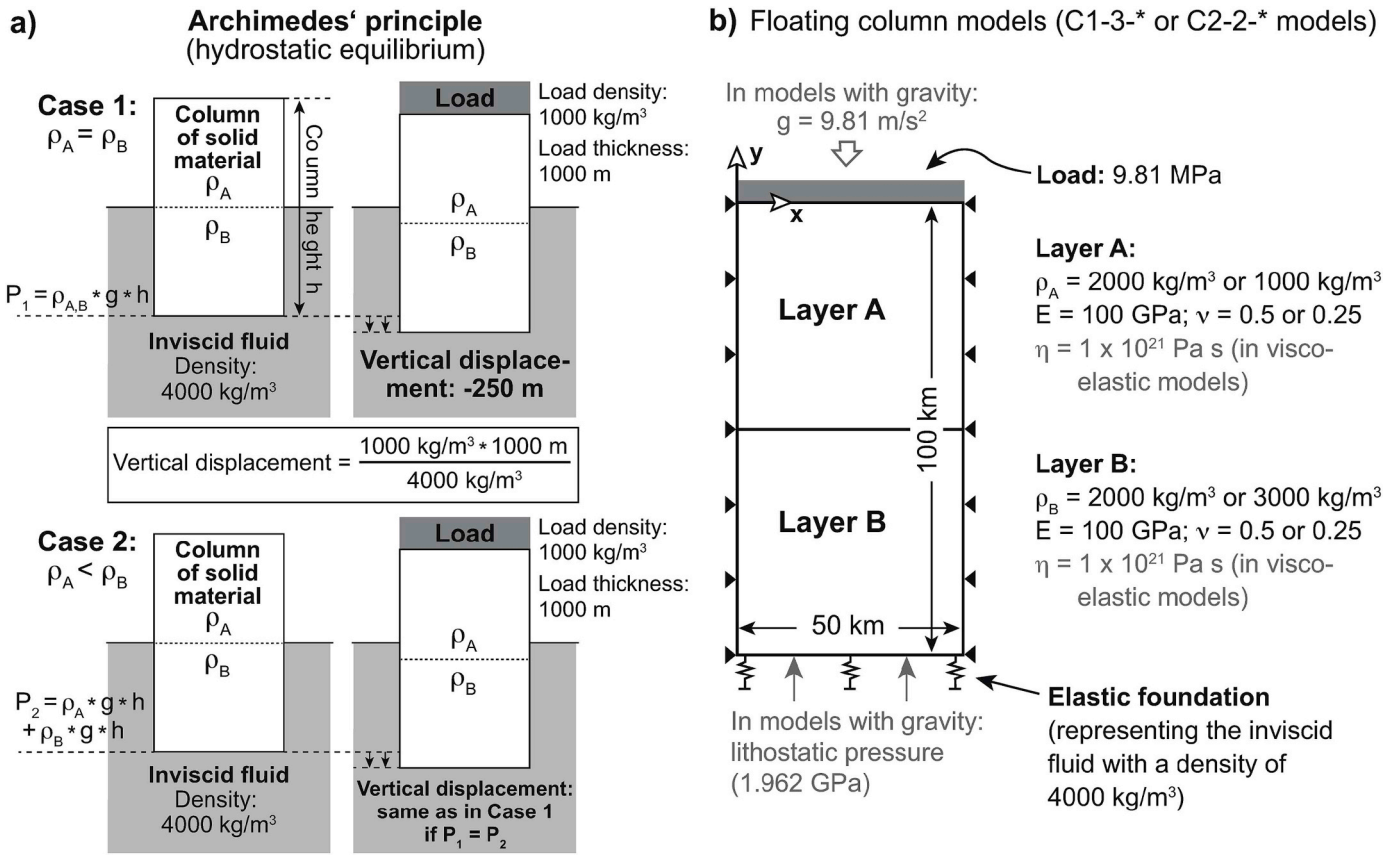

Fig. 4. Principle and setup of the floating column models. a) Sketch illustrating Archimedes' principle for a column of solid material floating on an inviscid fluid. When the initial hydrostatic equilibrium is disturbed, the column is displaced by an amount that can be calculated from the load density times the load thickness divided by the density of the inviscid fluid. Note that the vertical displacement does not depend on the density structure of the solid column as long as the column weight and hence the pressure P at the column bottom does not change (i.e. $P_1 = P_2$). b) Setup of the models with a column floating on an inviscid fluid. Names of models with different densities in Layers A and B start with C1-3; models with the same density in Layer A and B have names starting with C2-2. The star (*) denotes further additions (see Table 1). Abbreviations are ρ density, *E* Young's modulus, *ν* Poisson's ratio, *η* viscosity and *g* acceleration due to gravity (here: standard value of 9.81 m/s^2). At the beginning of each model run, the column is in isostatic equilibrium. This initial equilibrium is then disturbed by instantaneous loading of the column. Black triangles indicate that the model sides are fixed in the horizontal direction. Note that the model bottom does not need to be fixed to in the horizontal direction; due to the boundary conditions at the model sides and the fact that the load is applied across the entire column width, the model bottom only moves in the vertical direction. In models with NLGEOM, the only elastic foundation is applied at the model bottom to simulate the inviscid fluid; the foundation stiffness is calculated from the absolute density (4000 kg/m^3) times acceleration due to gravity. In models with elastic foundations at all material boundaries, the density contrast (variable) between 4000 kg/m^3 and the density of Layer B is used. All models have the same mesh with 500 × 500 m large linear rectangular plane strain elements (incompressible material: CPE4H; compressible material; CPE4). To minimize the deformation caused solely by applying gravity to a compressible material, the experiments were run with an initial geostatic stress field and geostatic step (cf. ABAQUS 6.14 documentation; for consistency, this step sequence was also applied to models with incompressible materials). The resulting initial compression due to gravity is less than 1 mm in all compressible models. Starting the analysis with a geostatic step does not influence the model behaviour during loading; if the *Geostatic step is replaced by a *Static step, identical results are obtained (Fig. S10). In models with elastic material, the load is applied instantaneously in the next model step (*Static; duration: 1 s). In models with viscoelastic materials, an additional step (*Visco; 10 ka) is included after application of gravity to allow relaxation of stresses induced by the application of gravity. The load is applied at the beginning of the subsequent step (*Visco; 10 ka).

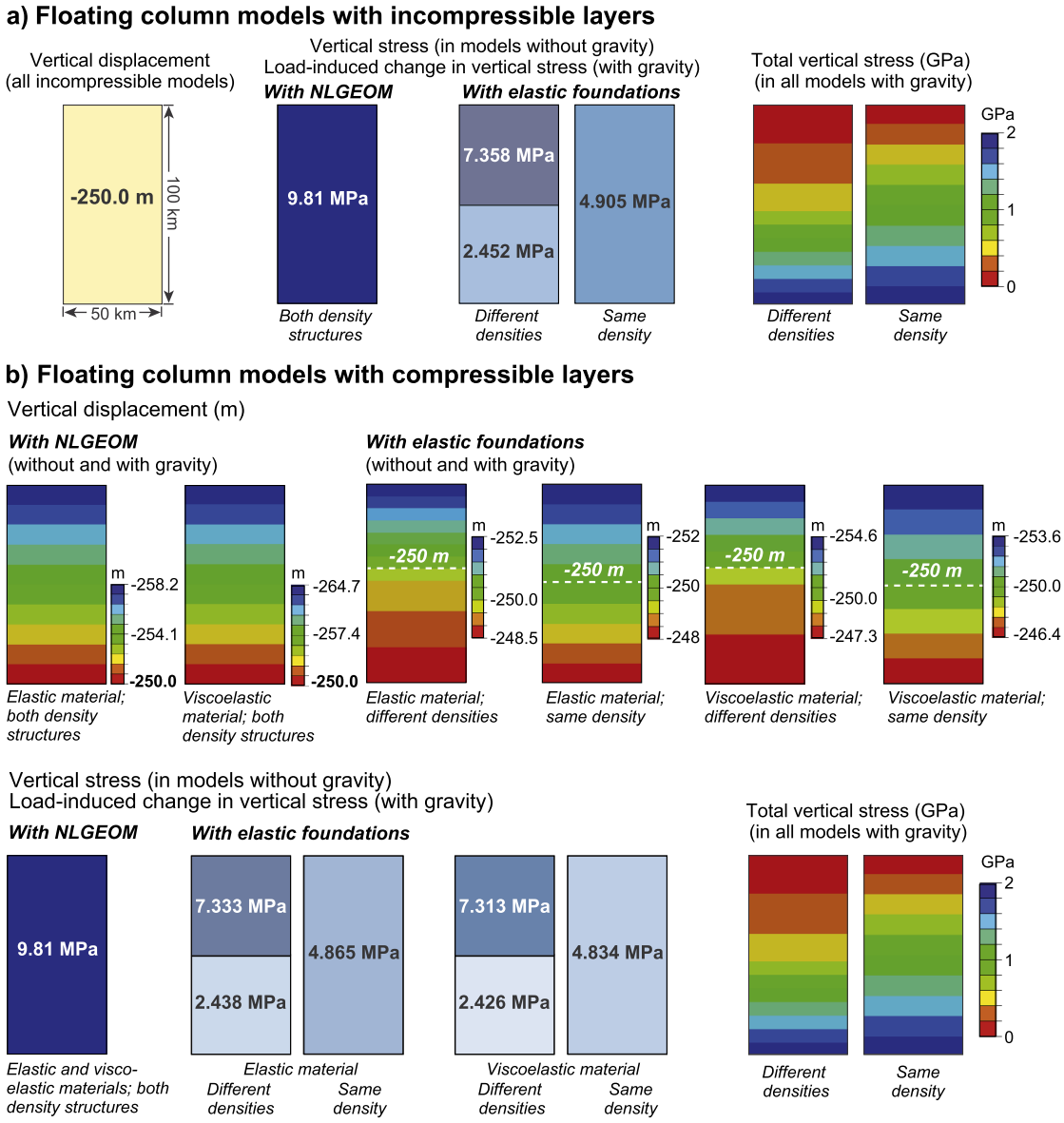

Fig. 5. Results from models with a column of solid material floating on an inviscid fluid (Fig. 4; Table 1). The latter is represented by an elastic foundation at the bottom of the model. (a) Vertical displacement and stresses in models with incompressible materials. (b) Vertical displacements and stresses in models with compressible material. All stress fields are shown as obtained from ABAQUS, i.e. stress values from models with elastic foundations at all material boundaries are shown without post-processing after Wu (2004). See text for details.

solution (Fig. 2a and b; Table 2). At the edge of the load, both model types show maximum deviations from the inverse Fourier transformation between −2.5 and 4.2 m (Fig. 2c and d), which are caused by the Gibbs effect. Across the entire model surface, the difference between models Haskell_N and Haskell_E is less than 1 m (Fig. S5a). Similar results are obtained for element edge lengths of 50 and 100 km, respectively, except at the edge of the load where the deviation from the analytical solution and the difference between the models increases (Fig. S5b, c).

The two other models (Fig. 2e and f) show completely different results and do not agree with the analytical solution. In the model Haskell_noNE (no elastic foundation, no NLGEOM), the vertical surface displacements are an order of magnitude too high and increase non-linearly through time (Fig. 2e, Table 2). The model surface shows the typical sinking of the load with time that is expected for the small-displacement approximation (Williams and Richardson, 1991; Wu, 1992, 2004). Notably, also the model Haskell_N + E (with NLGEOM and elastic foundation) does not yield correct results; the vertical displacements are up to ~50% too low (Fig. 2f; Table 2).

With respect to the vertical stress, models Haskell_N and Haskell_noNE show the correct stress change of 15 MPa beneath the load without post-processing (Fig. S6a, b); in models Haskell_E and Haskell_N + E, the stress field is disturbed by the elastic foundations but post-processing according to Wu (2004) yields the correct vertical stress field (Fig. S6c, d). For an evaluation of the horizontal and shear stress fields as well as the horizontal displacement of the model surface see

Figures S7-S9, respectively.

3.1.2. Setup and results of viscoelastic half-space models with loading and unloading

In the second model setup (Fig. 1b), the density is changed to 3400 kg/m^3 and instantaneous removal of the load is added. The respective ABAQUS model consists of six steps. The first four steps are identical with the Haskell-type models, except that the fourth step now lasts 16000 a. In the fifth step (*Visco; duration: 1 s), the load is removed and the elastic response is computed. Note that it is irrelevant for the calculation of the elastic response if a *Static step or a *Visco step is used, as long as the length of the latter is short with respect to the timescale of the viscous deformation; the use of a *Visco step ensures the continuity of the viscoelastic flow in the model, which is not considered in a *Static step. The sixth step (*Visco) lasts 16 ka and yields the long-term response to unloading.

Again, models Wu92-Fig2_N (with NLGEOM, no elastic foundation) and Wu92-Fig2_E (no NLGEOM, with elastic foundation) show vertical surface displacements after loading that differ by less than 1% from the solution obtained by inverse Fourier transformation (Fig. 3a and b; Table 3). Both models also show similar results after unloading (Table 3; Fig. 3a–c). For the time period 16–18 ka, the results agree (based on visual inspection) with the diagram shown in Wu (1992; his Fig. 2b). Between 18 and 24 ka, the vertical displacements in both models differ from Wu (1992)'s diagram by up to ~30 m, with the maximum deviation near the edge of the load. Notably, both models do not show a complete return to a horizontal surface at 32 ka, as depicted in Wu (1992; his Fig. 2b). Instead, vertical displacements of ± ~40 m still occur near the edge of the former load (Fig. 3a and b). This may be a response to the singularity at the edge of the Heaviside load. Another reason may be an incomplete stress relaxation before unloading, as Wu (1992) observed for power-law viscosities. Following Wu (1992), we show a semi-log plot of the remaining uplift versus model time (Fig. 3d), which reveals that the relaxation times at the x-coordinates 0, 550 and 750 km are 3.6, 4.8 and 6.0 ka, respectively. While the relaxation time at x = 0 km is close to the value of 3.3 ka obtained by Wu (1992), the other relaxation times are higher than the ones given in Wu (1992; 3.9 and 4.5 ka).

The model Wu92-Fig2_noNE (no NLGEOM, no elastic foundation) first shows the continuous sinking of the load (Fig. 3e). Removal of the load leads to uplift of the surface (565 m at x = 0; Table 3) to a position, where it remains until 32 ka (Fig. 3e). The model Wu92-Fig2_N + E (with NLGEOM and elastic foundation) (Fig. 3f) shows a similar temporal evolution as the model without NLGEOM (Wu92-Fig2_E) but the amount of subsidence and uplift is too low by up to ~50%.

3.2. Models of columns floating on an inviscid fluid - the effect of using elastic foundations on modelled displacement and stress fields

According to Wu (1992, 2004) and other authors (e.g. Lund, 2005; Steffen et al., 2006; Steffen, 2013), elastic foundations affect only the stresses but not the displacement field. Obtaining an undisturbed displacement field is particularly important when considering that it is required to post-process the ABAQUS stress output (see Section 2). To compare the displacement and stress fields obtained with and without NLGEOM, we use models representing a column of solid material floating on an inviscid fluid (Archimedes' principle; Fig. 4a). By applying a load to the column top, the initial hydrostatic equilibrium is disturbed and the column moves to a new equilibrium position. The displacement of the column bottom can be calculated from the product of load density and thickness divided by the density of the inviscid fluid (Fig. 4a) (Turcotte and Schubert, 2002). This setup represents the simplest form of isostatic adjustment following the application of a load (e.g. Watts, 2001). As the system behaviour is dominated by restoring forces, it is ideally suited to evaluate if the two approaches can correctly calculate these forces, the resulting isostatic displacement and the stress field. Note that shear stresses between column and fluid, lateral flow and other processes are deliberately not considered to keep the model simple. To allow an easy comparison with the analytical solution (Fig. 4a), we use a load density of 1000 kg/m^3, a load thickness of 1000 m and a density of the inviscid fluid of 4000 kg/m^3. With these values, the expected displacement of the model bottom is 250 m. Importantly, the displacement of the bottom does not depend on the density structure of the model as long as the column weight does not change (Fig. 4a). We will use this fact when evaluating the two different approaches against each other. The vertical stress in the model should be equal to the applied load (9.81 MPa).

The setup of the floating column models is depicted in Fig. 4b. In different experiments, the column is composed either of one 100-km-thick layer with a density of 2000 kg/m^3 or of two 50-km-thick layers with densities of 1000 and 3000 kg/m^3, respectively (Fig. 4b). In models without NLGEOM, elastic foundations (= density contrast x gravitational acceleration) are applied at all material boundaries. In models with NLGEOM, the only elastic foundation is applied at the model bottom to simulate the inviscid fluid. Using this setup, we ran models with and without gravity using incompressible and compressible as well as elastic and viscoelastic materials, respectively (Table 1; see Fig. 4b for rheological parameters and a description of the used ABAQUS analysis steps).

Results from models with incompressible elastic or viscoelastic material consistently show that the entire column is displaced by −250 m at the end of the loading step (Fig. 5a). There are no differences between models with and without internal elastic foundations or between models with different density structures. In NLGEOM models without gravity, the vertical stress is equivalent to the applied load (9.81 MPa) and does not need post-processing. In the corresponding models without NLGEOM, the stress is perturbed by the elastic foundations (Fig. 5a) but adding a value of 250 m times 9.81 m/s^2 times layer density to the stress output yields the correct constant value of 9.81 MPa. In models with gravity, the magnitude of the load is added to the vertical stress; as the former is much smaller than the latter except near the surface, models with and without NLGEOM show similar vertical stress fields. When calculating the stress change induced by the load, the same values as for models without gravity are obtained (Fig. 5a).

The effect of the internal elastic foundations becomes discernible for compressible elastic and viscoelastic materials (Fig. 5b). Models with NLGEOM show the correct displacement (−250 m) of the model bottom for both density structures. In the elastic model, the surface is displaced by −258.2 m; the viscoelastic model shows the same elastic response and a value of −264.7 m at the end of the experiment. In models with elastic foundations at the base and at all internal material boundaries, the bottom is displaced by different amounts but always less than 250 m; the 250 m isoline is located at different levels within the model (Fig. 5b). This implies that the displacement field in models with internal elastic foundations depends on the density structure, which is a non-physical behaviour and in contradiction with the theoretical consideration (cf. Fig. 4a). In other words, elastic foundations in the model interior and at the model surface perturb the vertical displacement field. As they take up part of the applied pressure, only a portion of the load is transferred to the model bottom, leading to less subsidence than expected. The perturbed displacement field poses a serious problem for post-processing the stress output, which is best illustrated for the models without gravity: depending on the density

structure, models without NLGEOM yield one or two constant values for the vertical stress, respectively (Fig. 5b). To correct the values, one would need to add a value obtained from the product of vertical displacement times 9.81 m/s^2 times layer density. As the displacement varies with depth, however, the post-processed stress field would also be depth-dependent instead of showing a constant value for the whole model.

To complement our analysis, we computed models with both elastic foundations and NLGEOM. These models yielded the same results as the models with elastic foundations only. This is in marked contrast to the results obtained from the Haskell- and Wu92-Fig2a-type models, where the combination of NLGEOM and elastic foundations yielded only a portion of the theoretically predicted displacement. These differences result from the change in the boundary condition at the model bottom, which is fixed in the Haskell- and Wu92-Fig2a-type models but free to move in the vertical direction in the column models, and from the fact that the load is applied over the entire column width.

4. Discussion

Our results show that models with NLGEOM (but without elastic foundations) and models with elastic foundations (but without NLGEOM) yield similar results for incompressible materials. The computational efficiency is similar for both model types, with the latter requiring ~90% of the computational time of the former. Our results demonstrate that ABAQUS is able to compute restoring forces in a Lagrangian, geometrically non-linear analysis without adding internal elastic foundations. Given that NLGEOM is the recommended procedure for quasi-static analyses (ABAQUS 6.14 documentation), it is rather surprising that the use of the small-displacement approach (i.e. no NLGEOM) can be compensated (at least for incompressible materials) by including elastic foundations. The reason may be that the computed quantities are referenced to the initial nodal positions in the small-displacement approach. Although not strictly comparable, this referencing to the initial mesh geometry also occurs in the Eulerian formulation of the equations of motion (eq. (1)), which was the starting point for Wu (1992, 2004). This equivalence in nodal referencing in the Eulerian formulation and small-displacement approach explains a) the need for separate handling of pre-stress advection and b) why Wu (1992, 2004) obtains – for incompressible materials – correct results. In contrast, the use of elastic foundations in an NLGEOM analysis is not only unnecessary but produces wrong results (Figs. 2, 3 and 5).

When using elastic foundations in small-displacement models with compressible materials, the approach fails. In this case, models with elastic foundations show a non-physical behaviour and a significant perturbation of the displacement field (Fig. 5b). This finding is consistent with Bängtsson and Lund (2008), who showed that the incorporation of the pre-stress advection term as a boundary condition (i.e. as an elastic foundation) is only valid for incompressible solids and that for compressible materials stress, strain and displacements are disturbed. Bängtsson and Lund (2008) still claim, however, that *"the buoyancy term needs to be computed by coupling to external computations"*. Our results show that such external iterative computations of the restoring forces are not necessary if the analysis is run with NLGEOM. Notably, also internal buoyancy forces due to material compressibility are considered by ABAQUS when implementing gravity via the load type *Dload (type = gravity) in an NLGEOM analysis (see Fig. S11; for details, verification models and examples see the ABAQUS documentation). The large-displacement approach can also be applied to calculate restoring forces arising at material boundaries that are initially inclined (e.g. Lang et al., 2014; Naliboff et al., 2012; Nikolinakou et al., 2014) or become inclined during the model run (e.g. Hampel et al., 2009; Li and Urai, 2016a). Omitting internal elastic foundations also allows considering negative density contrasts between layers, which is required, for example, for modelling of salt diapirs (Li and Urai, 2016b; Nikolinakou et al., 2014) and their behaviour during the advance and retreat of ice sheets (Lang et al., 2014).

5. Conclusions

Based on theoretical considerations and finite-element experiments, we show that the apparent necessity for elastic foundations to correctly model restoring forces arises from an Eulerian formulation of the equation of motion and the use of the small-displacement approach in the finite-element models. If models are run as non-linear geometry analyses, ABAQUS correctly calculates load-induced restoring forces, displacements and stresses. The two approaches (elastic foundations or NLGEOM) yield equivalent results only for incompressible materials. For compressible materials, internal elastic foundations perturb both displacements and stresses. This poses a problem for post-processing the stress output, which relies on the assumption that displacements are not affected by the elastic foundations. Models with NLGEOM yield correct displacement and stress fields without the need of post-processing. If elastic foundations are included in an NLGEOM model, the results depend on the density structure and the boundary condition at the model bottom. Our findings imply that models requiring isostatic effects should be run with NLGEOM because this makes the simulation of restoring forces by elastic foundations obsolete and avoids undesired effects on stresses and displacements. The described procedures to implement gravity, isostasy, flexure and rebound are not restricted to GIA modelling but can also be used in other geodynamic models simulating, for example, deformation on lithospheric or crustal scale or in subduction zones.

Acknowledgements

We thank four anonymous reviewers for their reviews that improved the manuscript. A.H. would like to thank the Simulia Support and particularly Fengming Zhou for inspiring discussions during the Simulia Community Conference in Berlin (2015) and thoughtful suggestions to test the two approaches. We also thank Raimar Wulkenhaar (Mathematisches Institut der Westfälischen Wilhelms-Universität Münster) for help and discussion on the inverse Fourier transformation. ABAQUS input files are available from the corresponding author (for templates of input files see Appendix A).

Appendix A. Templates for ABAQUS input files with NLGEOM

A.1 Template for an NLGEOM model without gravity

```
*Heading
** Job name: job-name
** PARTS
*Part, name=part-name
*End Part
** ASSEMBLY
*Assembly, name=assembly-name
*Instance, name=instance.name, part= part-name
*Node
*Element, type=element-type
**
** MATERIALS
*Material, name=name-material
*Density
*Elastic
** optional for a viscoelastic material:
*Creep
**
** INTERACTIONS
*Foundation
** ----------------------------------------------------------------
**
** STEP: Step-1
**
** for elastic models:
*Step, name=Step-1, nlgeom=YES
*Static
**
** for viscoelastic models:
*Step, name=Step-1, nlgeom=YES, inc=100000
*Visco, cetol=0.001
**
** BOUNDARY CONDITIONS
*Boundary
**
** LOADS
** load applied on model surface
*Dsload
**
** OUTPUT REQUESTS
*Output, field
*Node Output
*Output, history
*Energy Output
**
*End Step
```

A.2 Template for an NLGEOM model with gravity

Note: The definition of an initial stress field and the steps 1–3 are optional but recommended to minimize deformation that occurs solely in response the application of gravity to the model.

```
*Heading
** Job name: job-name
** PARTS
*Part, name=part-name
*End Part
** ASSEMBLY
*Assembly, name=assembly-name
*Instance, name=instance.name, part= part-name
*Node
*Element, type=element-type
**
** MATERIALS
*Material, name=name-material
*Density
*Elastic
** optional for a viscoelastic material:
*Creep
**
** PREDEFINED FIELDS
*Initial Conditions, type=STRESS, GEOSTATIC
**
** INTERACTIONS
*Foundation
** ----------------------------------------------------------------
**
** STEP: Step-1
**
*Step, name=Step-1, nlgeom=YES
*Geostatic
** or as an alternative:
*Step, name=Step-1, nlgeom=YES
*Static
**
** BOUNDARY CONDITIONS
** fix whole model in x- and y-direction
*Boundary
whole-model, 1, 1
whole-model, 2, 2
**
** LOADS
*Dload
whole-model, GRAV, 9.81, 0., -1.
** define lithostatic pressure at model bottom
*Dsload
**
** OUTPUT REQUESTS
*Output, field
*Node Output
*Output, history
```

```
*Energy Output
*End Step
* ----------------------------------------------------------------
** STEP: Step-2:
**
*Step, name=Step-2, nlgeom=YES
*Static
**
** BOUNDARY CONDITIONS
**
** deactivate previous boundary condition that whole
** model is fixed and define new boundary conditions
**
*Boundary, op=NEW
**
** OUTPUT REQUESTS
*Output, field
*Node Output
*Output, history
*Energy Output
**
*End Step
** ----------------------------------------------------------------
** STEP: Step-3: optional equilibration step for
** viscoelastic materials
**
*Step, name=Step-3, nlgeom=YES, inc=10000
*Visco, cetol=0.001
**
** OUTPUT REQUESTS
*Output, field
*Node Output
*Output, history
*Energy Output
**
*End Step
** ----------------------------------------------------------------
** STEP: Step-4
**
*Step, name=Step-4, nlgeom=YES, inc=100000
*Visco, cetol=0.001
**
** LOADS
** load applied on model surface
*Dsload
**
** OUTPUT REQUESTS
*Output, field
*Node Output
*Output, history
*Energy Output
**
*End Step
```

Appendix B. Supplementary data

Supplementary data related to this article can be found at https://doi.org/10.1016/j.cageo.2018.08.002.

References

ABAQUS 6.14 Documentation, Dassault Systèmes Simulia Corp., Johnston, Rhode Island, USA.

Bängtsson, E., Lund, B., 2008. A comparison between two solution techniques to solve the equations of glacially induced deformation of an elastic Earth. Int. J. Numer. Meth. Eng. 75, 479–502.

Bird, P., 1978. Finite element modeling of lithosphere deformation: the Zagros collision orogeny. Tectonophysics 50, 307–336.

Cathles, L.M., 1975. The Viscosity of the Earth's Mantle. Princeton University Press, Princeton, U.S.A., pp. 390pp.

Ellis, S., Beavan, J., Eberhart-Phillips, D., Stöckhert, B., 2006. Simplified models of the Alpine fault seismic cycle: stress transfer in the mid-crust. Geophys. J. Int. 166, 386–402.

Fischer, K.D., 2001. Dreidimensionale Modellierung der synorogenen Entwicklung des Variszischen Vorlandbeckens mit der Finite-Elemente-Methode. Dissertation, Friedrich-Schiller-Universität Jena, Jena, Germany, pp. 168.

Fischer, K.D., Jahr, T., Jentzsch, G., 2004. Evolution of the Variscan foreland-basin: modelling the interactions between tectonics and surface processes. Phys. Chem. Earth 29, 665–671.

Fourel, L., Goes, S., Morra, G., 2014. The role of elasticity in slab bending. G-cubed 15, 4507–4525.

Hampel, A., Hetzel, R., 2006. Response of normal faults to glacial-interglacial fluctuations of ice and water masses on Earth's surface. J. Geophys. Res. 111, B06406. https://doi.org/10.1029/2005JB004124.

Hampel, A., Hetzel, R., Densmore, A.L., 2007. Postglacial slip rate increase on the Teton normal fault, northern Basin and Range Province, caused by melting of the Yellowstone ice cap and deglaciation of the Teton Range? Geology 35, 1107–1110.

Hampel, A., Hetzel, R., Maniatis, G., Karow, T., 2009. Three-dimensional numerical modeling of slip rate variations on normal and thrust fault arrays during ice cap growth and melting. J. Geophys. Res. 114, B08406. https://doi.org/10.1029/2008JB006113.

Hampel, A., Karow, T., Maniatis, G., Hetzel, R., 2010. Slip rate variations on faults during glacial loading and postglacial unloading: implications for the viscosity structure of the lithosphere. In: In: Pascal, C., Stewart, I.S., Vermeersen, B.L.A. (Eds.), Neotectonics, Seismicity and Stress in Glaciated Regions, vol. 167. Journal of the Geological Society London, pp. 385–399.

Haskell, N.A., 1936. The motion of a viscous fluid under a surface load. Part II. J. Appl. Phys. 7, 56–61.

Henk, A., 2006. Stress and strain during fault-controlled lithospheric extension - insights from numerical experiments. Tectonophysics 415, 39–55.

Hergert, T., Heidbach, O., Reiter, K., Giger, S.B., Marschall, P., 2015. Stress field sensitivity analysis in a sedimentary sequence of the Alpine foreland, northern Switzerland. Solid Earth 6, 533–552.

Hetzel, R., Hampel, A., 2005. Slip rate variations on normal faults during glacial-interglacial changes in surface loads. Nature 435, 81–84.

King, G., Ellis, M., 1990. The origin of large local uplift in extensional regions. Nature 348, 689–693.

Kurfeß, D., Heidbach, O., 2009. CASQUS: a new simulation tool for coupled 3D finite element modeling of tectonic and surface processes based on ABAQUS™ and CASCADE. Comput. Geosci. 35, 1959–1967.

Lang, J., Hampel, A., Brandes, C., Winsemann, J., 2014. Response of salt structures to ice-sheet loading: implications for ice-marginal and subglacial processes. Quat. Sci. Rev. 101, 217–233.

Lester, R., Lavier, L.L., McIntosh, K., Van Avendonk, H.J.A., Wu, F., 2012. Active extension in Taiwan's precollision zone: a new model of plate bending in continental crust. Geology 40, 831–834.

Li, S.-Y., Urai, J.L., 2016a. Numerical modelling of gravitational sinking of anhydrite stringers in salt (at rest). Boll. Geofis. Teor. Appl. 57, 233–246.

Li, S.-Y., Urai, J.L., 2016b. Rheology of rock salt for salt tectonics modeling. Petrol. Sci. 13, 712–724.

Love, A.E.H., 1911. Some Problems of Geodynamics. Cambridge University Press, Cambridge, UK 180pp.

Lund, B., 2005. Effects of Deglaciation on the Crustal Stress Field and Implications for Endglacial Faulting: a Parametric Study of Simple Earth and Ice Models. Svensk Kärnbränslehantering AB, Stockholm, Sweden, pp. 68 Technical Report TR-05-04.

Martin-Velazquez, S., de Vicente, G., 2012. The role of lithospheric heterogeneities in the location of the Cenozoic intraplate deformation of Iberia from finite element modeling. Tectonics 31, TC1009. https://doi.org/10.1029/2011TC002954.

McMullen Jr., R.J., Hodge, D.S., Cozzarelli, F.A., 1981. A technique for incorporating geothermal gradients and nonlinear creep into lithospheric flexure models. J. Geophys. Res. 86, 1745–1753.

Musiol, S., Holohan, E.P., Cailleau, B., Platz, T., Dumke, A., Walter, T.R., Williams, D.A., van Gasselt, S., 2016. Lithospheric flexure and gravity spreading of Olympus Mons volcano, Mars. J. Geophys. Res. 121, 255–272.

Naliboff, J.B., Lithgow-Bertelloni, C., Ruff, L.J., de Koker, N., 2012. The effects of lithospheric thickness and density structure on Earth's stress field. Geophys. J. Int. 188, 1–17.

Nikolinakou, M.A., Hudec, M.R., Flemings, P.B., 2014. Comparison of evolutionary and static modeling of stresses around a salt diapir. Mar. Petrol. Geol. 537–545.

Schmidt, P., Lund, B., Hieronymus, C., 2012. Implementation of the glacial rebound prestress advection correction in general-purpose finite element analysis software: springs versus foundations. Comput. Geosci. 40, 97–106.

Schotman, H.H.A., Wu, P., Vermeersen, L.L.A., 2008. Regional perturbations in a global background model of glacial isostasy. Phys. Earth Planet. In. 171, 323–335.

Schotman, H.H.A., Vermeersen, L.L.A., Wu, P., Drury, M.R., de Bresser, J.H.P., 2009. Constraints on shallow low-viscosity zones in Northern Europe from future GOCE gravity data. Geophys. J. Int. 178, 65–84.

Steffen, R., 2013. The Influence on Glacial Isostatic Adjustment on Intraplate Seismicity in Northeastern Canada. Ph.D. thesis. University of Calgary, Calgary, Canada 204pp.

Steffen, H., Kaufmann, G., Wu, P., 2006. Three-dimensional finite-element modeling of the glacial isostatic adjustment in Fennoscandia. Earth Planet Sci. Lett. 250, 358–375.

Steffen, R., Wu, P., Steffen, H., Eaton, D.W., 2014a. The effect of earth rheology and ice-sheet size on fault-slip and magnitude of postglacial earthquakes. Earth Planet Sci. Lett. 388, 71–80.

Steffen, R., Steffen, H., Wu, P., Eaton, D.W., 2014b. Stress and fault parameters affecting fault slip magnitude and activation time during a glacial cycle. Tectonics 33, 1461–1476.

Turcotte, D.L., Schubert, G., 2002. Geodynamics, second ed. Cambridge University Press.

Turpeinen, H., Hampel, A., Karow, T., Maniatis, G., 2008. Effect of ice sheet growth and melting on the slip evolution of thrust faults. Earth Planet Sci. Lett. 269, 230–241.

van der Wal, W., Barnhoorn, A., Stocchi, P., Gradmann, S., Wu, P., Martyn Drury, M., Vermeersen, B., 2013. Glacial isostatic adjustment model with composite 3-D Earth rheology for Fennoscandia. Geophys. J. Int. 194, 61–77.

Wang, H., Wu, P., 2006. Effects of lateral variations in lithospheric thickness and mantle viscosity on glacially induced relative sea levels and long wavelength gravity field in a spherical, self-gravitating Maxwell Earth. Earth Planet Sci. Lett. 249, 368–383.

Watts, A.B., 2001. Isostasy and Flexure of the Lithosphere. Cambridge University Press, Cambridge, U.K., pp. 458.

Wdowinski, S., Axen, G.J., 1992. Isostatic rebound due to tectonic denudation: a viscous flow model of a layered lithosphere. Tectonics 11, 303–315.

Williams, C.A., Richardson, R.M., 1991. A rheologically layered three-dimensional model of the san andreas fault in central and southern California. J. Geophys. Res. 96, 16597–16623.

Wolf, D., 1985. On Boussinesq's problem for Maxwell continua subject to an external gravity field. Geophys. J. Roy. Astron. Soc. 80, 275–279.

Wu, P., 1992. Deformation of an incompressible viscoelastic flat earth with power-law creep: a finite element approach. Geophys. J. Int. 108, 35–51.

Wu, P., 2004. Using commercial finite element packages for the study of earth deformations, sea levels and the state of stress. Geophys. J. Int. 158, 401–408.

Wu, P., 2005. Effects of lateral variations in lithospheric thickness and mantle viscosity on glacially induced surface motion in Laurentia. Earth Planet Sci. Lett. 235, 549–563.

Wu, P., Johnston, P., 1998. Validity of using flat-earth finite element models in the study of postglacial rebound. In: Wu, P. (Ed.), Dynamics of the Ice Age Earth: a Modern Perspective. Trans Tech Pub., Zurich, Switzerland, pp. 191–202.